Effect of Pressure on the Vibrational Structure of Insensitive Energetic Material 5-Nitro-2,4-dihydro-1,2,4-triazole-3-one

Reiko I. Hiyoshi,*,† Yuji Kohno,*,‡ Osamu Takahashi,§ Jun Nakamura,† Yoshitaka Yamaguchi,‡ Shinya Matsumoto,|| Nagao Azuma,⊥ and Kazuyoshi Ueda‡

Explosion Investigation Section, National Research Institute of Police Science, Kashiwanoha 6-3-1, Kashiwa, Chiba 277-0882, Japan, Department of Materials Chemistry, Graduate School of Engineering, Yokohama National University, Tokiwadai 79-5, Hodogaya-ku, Yokohama, Kanagawa 240-8501, Japan, Department of Chemistry, Graduate School of Science, Hiroshima University, Kagamiyama 1-3-1, Higashi-Hiroshima 739-8526, Japan, Faculty of Education and Human Sciences, Yokohama National University, Tokiwadai 79-2, Hodogaya-ku, Yokohama, Kanagawa 240-8501, Japan, and Department of Chemistry, Faculty of Science, Ehime University, Bunkyo-cho 2-5, Matsuyama 790-8577, Japan

Received: May 23, 2006

The Raman spectra of α form 5-nitro-2,4-dihydro-1,2,4-triazole-3-one (α-NTO, space group $P\bar{1}$) were measured in a high-pressure vessel diamond anvil cell (DAC). The pressure was increased to 27.6 GPa. In general, Raman bands show a blue shift because of the nature of the molecule packing as a high-pressure effect, but some particular bands exhibited a red shift, disappearance, split, or slight shifting in our experiments. Those red-shifting bands concerning hydrogen bonds, i.e., carbonyl and amino groups, are likely to work as a stabilizer against stimuli to the molecule or crystal. This stabilizing nature might characterize the insensitivity of NTO. Molecular dynamic (MD) calculations were performed to reveal the high-pressure effect of the α-NTO crystal. The coordinates of individual atoms in the crystal structure were obtained using X-ray diffraction analysis. The pressure dependence of the power spectra of the correlation functions of the C═O bond length in NTO was calculated. A unique high-pressure effect of the α-NTO crystal was found on the power spectra. The peak frequency in the power spectrum of the C═O stretching vibration exhibited a red shift with an increase in pressure to 10.0 GPa, while the peak intensity considerably decreased under the same pressure process, because this bond length increased with an increase in pressure to 10.0 GPa. At a pressure of >20.0 GPa, a blue shift appeared. These results of the MD calculations are in good agreement with our experimental data.

1. Introduction

5-Nitro-2,4-dihydro-1,2,4-triazole-3-one (NTO, Figure 1) is well-known as an insensitive but powerful explosive, and there are many reports about its thermal decomposition process,[1−4] explosion properties such as sensitivity and detonation velocity,[5−7] crystalline structure,[8−10] and computational chemistry.[11−18] However, the chemical structure at the initial stage of the detonation process is still unclear. It is generally believed that adiabatic compression occurs when shock waves propagate unreacted explosives, and the heat generated by fast compression brings about a chemical reaction. It is quite difficult to observe the chemical reaction of a detonation in situ, since a huge amount of energy (heat and light) and generated gas that becomes a blast wave are released. Several attempts to take real-time spectroscopic measurements have been reported,[19−22] but the chemical phenomenon of the detonation process has not been explained, because most measurements were carried out under mild conditions under which detonation could not occur, i.e., at a lower pressure and temperature, and shorter propagation time of the shock wave. Franken et al. used a laser-induced shock wave (∼2 ns, ∼5 GPa) as a perturbation to the NTO film and observed an unexpected new peak during the shock propagation and unusual shifts after the shock via coherent anti-Stokes Raman spectroscopy (CARS).[23] They pointed out a relationship between the spectral change and the pressure profile; i.e., the spectra changed as a function of the pressure value.

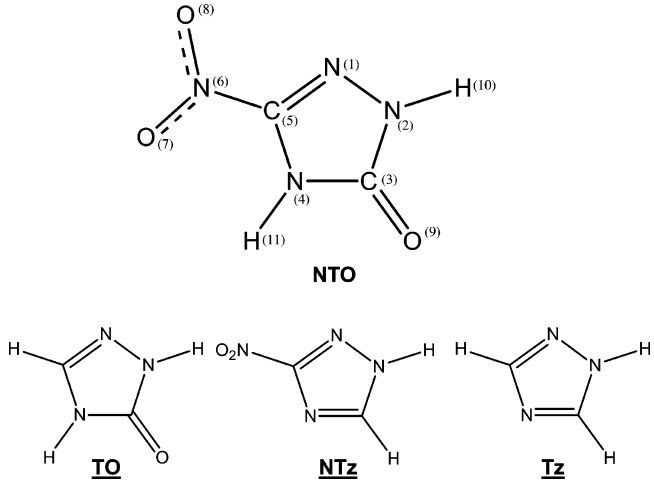

Figure 1. Molecules of the triazole group. Numbers on each atom of NTO correspond to numbers used in computational calculations.

* To whom correspondence should be addressed. R.I.H.: telephone, +81-4-7135-8001; fax, +81-4-7133-9169; e-mail, ichiki@nrips.go.jp. Y.K.: telephone, +81-22-217-5294; fax, +81-22-217-5324; e-mail, kohnoy@ynu.ac.jp.

† National Research Institute of Police Science.

‡ Graduate School of Engineering, Yokohama National University.

§ Hiroshima University.

|| Faculty of Education and Human Sciences, Yokohama National University.

⊥ Ehime University.

10.1021/jp063142+ CCC: $33.50
Published on Web 07/20/2006

The temperature at high pressure of the laser shock was estimated by Raman bandwidths. It was approximately 400 K, but no chemical reaction was observed within this short time duration.

In the study presented here, it was assumed that the structural change in a very fast region of the detonation process might be observed in the Raman spectra as an effect of the pressure before the adiabatic thermal effect. An experimental condition of this study such as static pressure will never take place in a real detonation process, but the pressure effect may bring about changes in the molecular structure or crystalline structure faster than the heat effect. The Raman spectra under high pressure presented the tendency of the reactivity of the sample in this work.

Static high pressure to the sample was introduced into the diamond anvil cell (DAC) with liquid pressure medium to generate a homogeneous pressure field. In this work, a very high static pressure of up to 27.6 GPa was applied to the sample in the DAC. Licht reported that NTO was not initiated by a ca. 5 GPa shock with a Card Gap test[24] but that NTO could be initiated by a booster charge. The detonation pressure of a booster charge is estimated to be 20−30 GPa, and therefore, we decided to achieve static pressure up to around 30 GPa.

The existence of two types of NTO polymorphs has been reported, α and β. The α form is stable at room temperature and is used in general applications. The α form is well-known as a twinned crystal and is usually obtained from ordinary recrystallization. The β form is recrystallized with only a special treatment. The crystalline structure of β-NTO determined by X-ray diffraction was reported.[10] Although α-NTO is the stable form, the difficulty of determining the crystal structure was proven as a result of twinning.[8] In the work presented here, only α-NTO was used due to the feasibility of the recrystallization and stability to light and humidity (the abbreviation for α-NTO is NTO in this paper).

When the Raman spectra of NTO were measured, the relative intensities of each Raman band vary depending on the direction of the crystal face to the laser beam due to the crystal twinning.[23] In our study, a very small piece of NTO crystal (∼50 μm) was used in the DAC, but it was impossible to control the orientation of the crystal in such a small area. The Raman spectral intensity pattern changed with every series of experiments depending on the direction of the crystal, but fortunately, the Raman frequencies did not change. We focused on the frequency shifts with compression in this study.

To evaluate the effect of the functional groups of NTO under high pressure, 1,2,4-triazole-3-one (TO), 3-nitro-1,2,4-triazole (NTz), and 1,2,4-triazole (Tz) were also investigated using the same experimental method as NTO. These three compounds have a similar five-membered ring as NTO, while nitro and/or carbonyl groups are missing in TO, NTz, and Tz (Figure 1).

Molecular dynamics (MD) simulations have been shown to be a valuable tool for revealing the mechanisms of various kinds of reactions and the thermodynamic properties of energetic materials at a variety of temperatures and pressures.[25−28] In a molecular dynamics study of NTO, crystal packing calculations of β-NTO were studied by Sorescu et al.[14] As mentioned above, NTO exists in two polymorphic modifications known as the α and β forms. The β crystal form is not stable and reverts to the α form after standing for several months. The α form is stable at room temperature and is used in general applications and analysis. However, there has been no study of the molecular dynamics of the α-NTO crystal. In particular, there have been no detailed molecular dynamics studies that would clarify the dynamic mechanism of the initial reaction step of the α-NTO crystal under high pressure (∼50.0 GPa). Therefore, we carried out molecular dynamics simulations with the α-NTO crystal to study the initial process before decomposition under high pressure (∼50.0 GPa). We attempted to determine the coordinates of individual atoms by using X-ray diffraction analysis to carry out molecular dynamics simulations with the α-NTO crystal.

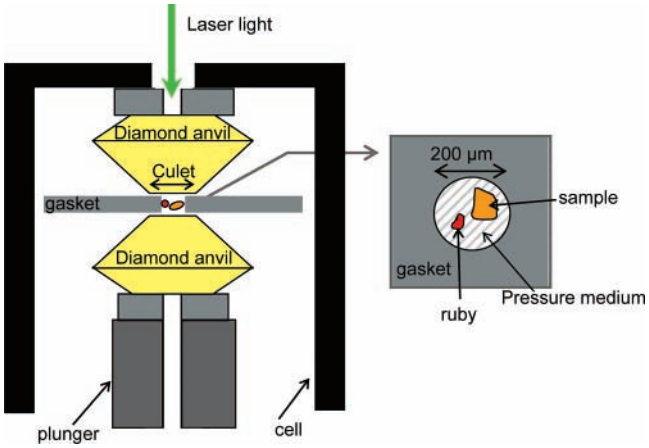

Figure 2. Cross-sectional view of the diamond anvil cell (DAC) and view of the sample chamber.

2. Experimental Section

A. Sample Preparation. NTO was synthesized by the method of Oxley,[29] with some improvements. NTO was recrystallized from distilled water. The NTO crystal was stored in a desiccator after filtration and crushed into small pieces before being measured.

TO was synthesized as described in our previous study.[30] NTz and Tz were purchased from Tokyo Kasei Kogyo Co., Ltd., and Wako Chemical Co., Ltd., respectively. All samples were recrystallized from distilled water in the same way as NTO.

B. High-Pressure Apparatus. The structure of DAC (Kyowa Seisakusho, SR-DAC-KYO3-3) is shown in Figure 2. Type Ia and Ib diamond anvils were chosen for Raman spectroscopy. The culet diameters of these diamond anvils were 0.6 and 1.0 mm and the heights 1.8 and 1.5 mm, respectively. To avoid a very strong Raman band of the diamond anvil around 1333 cm^{-1} as background, silicon carbide (SiC, moissanite) anvils were also used to investigate the 1200−1400 cm^{-1} region since dominant Raman bands of SiC are at 791 and 969 cm^{-1}. The diameter of the culet was 0.6 mm, and the height of the SiC anvil was 1.4 mm. Although SiC is a hard material, it is softer than a diamond; therefore, a pressure of ≤5 GPa could be achieved with SiC anvils, while diamond anvils could withstand a pressure of ca. 27.6 GPa in this study. It is said that the practical pressure of an ordinary booster is estimated to be 20−30 GPa, and therefore, the pressure range was set up from ambient pressure to ∼30 GPa in this study. All experimental pressure values are represented in gauge pressure.

Liquid paraffin was used as a pressure medium since its Raman signal was very weak compared to the signal of NTO. The Raman spectra were measured at least 30 min after the pressure loading to eliminate the inhomogeneity of the pressure in the sample chamber between diamond anvils. The thickness of the inserted stainless gasket was 200 μm, and the diameter of the sample hole on the gasket was 200 μm. A minute piece of ruby crystal (<100 μm in diameter) was confined with the sample to monitor the pressure of the sample chamber in the

TABLE 1: Force Constants of NTO at the B3LYP/6-311++G(d,p) Level

bond	k_b (kcal mol^{-1} Å^{-2})	l_0(equil. value) (Å)
N1−N2	386.73	1.35880
N2−N3	329.31	1.39760
C3−N4	337.55	1.40270
N4−C5	485.24	1.36577
C5−N1	568.70	1.29060
N2−H10	532.30	1.00861
C3−O9	868.89	1.20484
N4−H11	533.54	1.00913
C5−N6	272.34	1.45158
N6−O8	600.92	1.21504
N6−O7	619.77	1.23020
bond angle	**k_θ (kcal mol^{-1} rad^{-2})**	**θ_0(equil. value) (deg)**
N1−N2−C3	268.54	144.4491
N2−C3−N4	301.39	100.7090
C3−N4−C5	276.90	107.6890
N4−C5−N1	239.56	113.7550
C5−N1−N2	247.34	103.3800
H10−N2−N1	68.45	120.0560
O9−C3−N2	113.30	129.4760
H11−N4−C3	55.39	125.8900
N6−C5−N1	108.81	124.3370
O8−N6−C5	123.48	118.4710
O7−N6−C5	134.12	114.7140
O8−N6−O7	156.56	126.8150
C5−N4−H8	55.39	126.4210
N4−C3−O9	112.68	129.8100
C3−N2−H10	67.90	125.4770
N4−C5−N6	108.11	121.9080
dihedral angle	**k_Φ (kcal mol^{-1} rad^{-2})**	**n**	**δ (deg)**
N1−N2−C3−N4	21.46	2	180.0
N1−N2−C3−O9	18.39	2	180.0
N1−C5−N4−C3	14.63	2	180.0
N1−C5−N6−O8	5.19	2	180.0
N1−C5−N6−O7	6.07	2	180.0
N2−N1−C5−N4	44.97	2	180.0
N2−N1−C5−N6	18.88	2	180.0
N2−C3−N4−C5	25.19	2	180.0
N2−C3−N4−H11	5.81	2	180.0
C3−N2−N1−C5	28.33	2	180.0
C3−N4−C5−N6	16.81	2	180.0
N4−C5−N6−O8	7.13	2	180.0
N4−C5−N6−O7	7.64	2	180.0
C5−N1−N2−H10	6.05	2	180.0
H10−N2−C3−N4	5.81	2	180.0
H10−N2−C3−O9	4.61	2	180.0
O7−C3−N4−C5	19.90	2	180.0
O7−C3−N4−H11	5.45	2	180.0
H11−N4−C5−N1	6.53	2	180.0
H11−N4−C5−N6	5.16	2	180.0
improper torsion	**k_ω (kcal mol^{-1} rad^{-2})**	**ω_0 (deg)**
N2−N1−C3−H10	3.385	0.0
C3−N2−N4−O9	32.436	0.0
N4−C3−C5−H11	3.818	0.0
C5−N4−N1−N6	13.613	0.0
N6−C5−O8−O7	26.914	0.0

DAC on the basis of the ruby fluorescence scale following the method of Piermarini et al.[31]

C. Raman Spectroscopy. The Raman spectra were measured with a Nicolet Almega instrument (microscope mode) in the range of 100−3700 cm^{-1}. The laser wavelength was 532 nm (power of ∼1 mW at the sample stage) for excitation of both Ruby and NTO. The resolution of the Raman spectra was 2.2−2.5 cm^{-1}. The magnification of the long working distance objective lens was 50×.

All measurements were taken at room temperature (∼20 °C).

TABLE 2: Electrostatic Charges for the NTO Molecule Determined by the Merz−Kollman−Singh Procedure at the B3LYP/6-311++G(d,p) Level

atom	charge/|e|	atom	charge/|e|
N1	−0.408	O7	−0.430
N2	−0.142	O8	−0.369
C3	0.574	O9	−0.535 (−0.635)[a]
N4	−0.434	H10	0.328 (0.428)[a]
C5	0.391	H11	0.365
N6	0.660		

[a] Adjusted value.

D. Crystal Structure of α-NTO. A suitable single crystal of α-NTO was obtained by recrystallization from acetonitrile at room temperature and was mounted on glass fiber. Indexing was performed from three oscillations, which were exposed for 1.5 min using a Rigaku RAXIS-RAPID Imaging Plate diffractometer with graphite-monochromated Cu Kα radiation. The camera radius was 127.40 mm. Readout was performed in the 0.100 mm pixel mode. The data were collected on a Rigaku AFC-7R automated four-circle diffractometer with graphite-monochromated Mo Kα radiation, and measurements were carried out at −50 ± 2 °C using the $\omega-2\theta$ scan technique to a maximum 2θ value of 60.0°.

The structure was determined by direct methods (SIR 92)[32] and expanded using Fourier techniques.[33] The non-hydrogen atoms were refined anisotropically. Hydrogen atoms were located from difference Fourier maps and refined isotropically. Least-squares refinement was carried out using SHELXL-97.[34] All calculations were performed on an SGI Indy computer using the teXsan crystallographic software package of the Molecular Structure Corp.[35]

3. Computational Methods and Procedures

Molecular dynamics simulations were performed to investigate the pressure effects on the NTO crystal structure using CHARMM29.[37] All simulations were calculated for the α-NTO crystal at pressures ranging from 1 atm to 50.0 GPa.

A. Potential Function. The CHARMM29 potential energy function is expressed as follows

$$E = \sum k_b(l - l_0)^2 + \sum k_\theta(\theta - \theta_0)^2 + \sum \frac{k_\phi}{2}[1 + \cos(n\phi - \delta)] + \sum k_\omega(\omega - \omega_0)^2 + \sum_{\mathrm{excl}(i,j)=1} \sqrt{\epsilon_i^* \epsilon_j^*}\left\{\left[\frac{0.5(r_i^* + r_j^*)}{r_{ij}}\right]^{12} - 2\left[\frac{0.5(r_i^* + r_j^*)}{r_{ij}}\right]^{6}\right\} \mathrm{SW}(r_{ji}, r_{on}, r_{off}) + \sum_{\mathrm{excl}(i,j)=1} \frac{q_i q_j}{4\pi\epsilon_0 r_{ji}^2} \mathrm{SW}(r_{ji}, r_{on}, r_{off}) \quad (1)$$

where k_b, k_θ, k_Φ, and k_ω are the bond, angle, dihedral angle, and improper torsional angle force constants, respectively. The first two terms describe the intramolecular interactions between bonded atoms; the quantities $l - l_0$ and $\theta - \theta_0$ are the displacements from the equilibrium bond length and angle, respectively. The torsion energy term is a four-atom term based on the dihedral angle about an axis defined by the middle pair of atoms. The improper torsional term has been designed for the maintenance of planarity with regard to certain planar atoms with a quadratic distortion potential. The nonbonded interaction terms are van der Waals interactions and Coulombic interactions

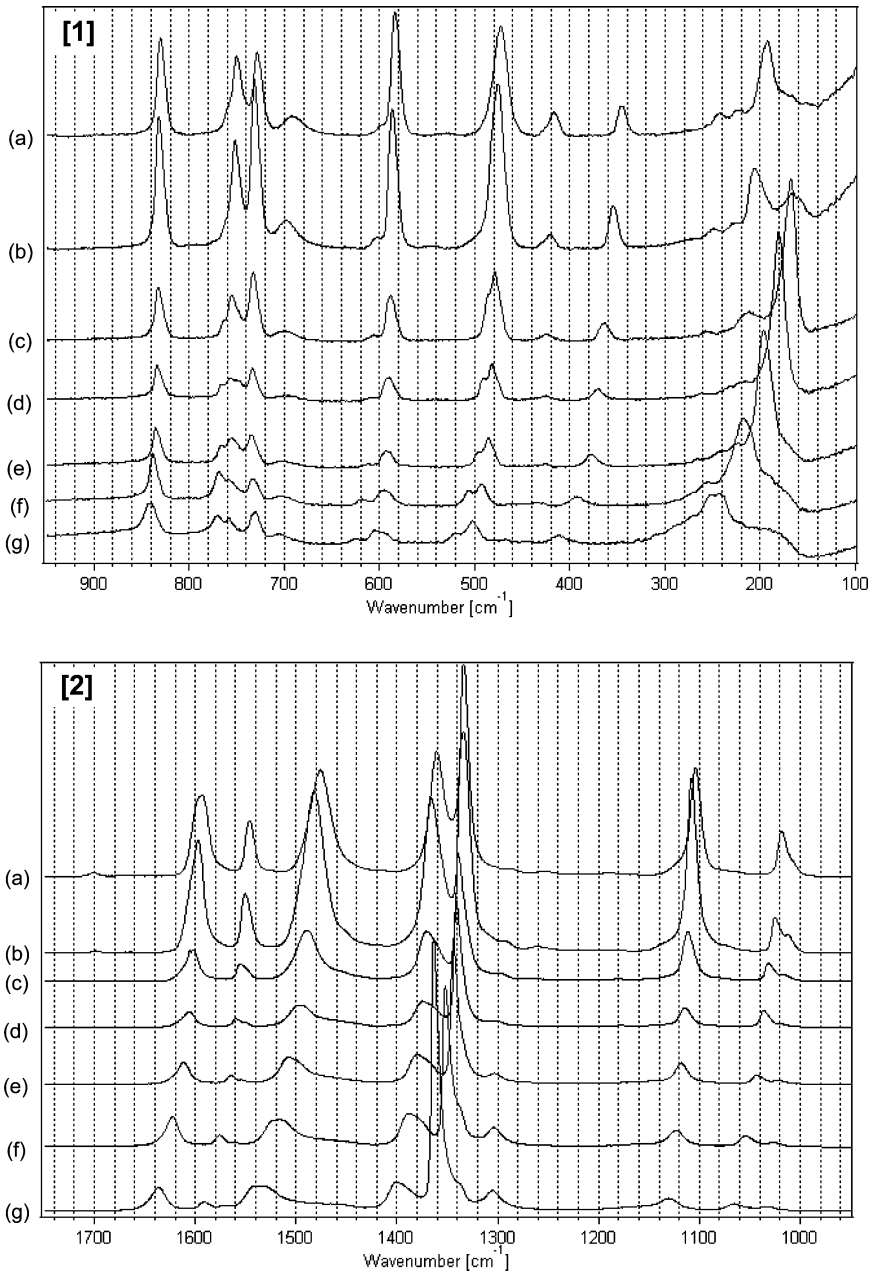

Figure 3. Effect of pressure on NTO in Raman spectra, in the low-pressure region under 10 GPa. **[1]** Low-frequency region and **[2]** high-frequency region: (a) 0.05, (b) 1.10, (c) 2.36, (d) 3.45, (e) 4.60, (f) 6.74, and (g) 9.75 GPa. Pressure values are represented as gauge pressure.

between the partial charges on the individual atoms, where r_{ij} is the distance between atoms i and j in a system and ϵ^*, r^*, and SW are the well depth, the position of the minimum in the Lennard-Jones potential, and a switching function,[37] respectively. The parameters for the nonbonded interaction terms are those used in CHARMM29. There is a role of the switching function in preventing this burden of various truncations. Long-range interactions were cut off between 8.5 and 9.0 Å by use of a switching function. SW is a switching function defined by Brooks et al.[37]

B. Force Constants and Partial Atomic Charges. In this work, we developed a CHARMM-type force field for NTO by using density functional theory (DFT) calculations. Especially, since there are no appropriate parameters for the C−NO_2 moiety of NTO in CHARMM29, density functional theory (DFT) calculations were performed with GAUSSIAN 98[38] at the B3LYP/6-311++G(d,p) level, with the Becke 3LYP(B3LYP) hybrid density functional with the 6-311++G(d,p) (split-valence plus diffuse functions plus d polarization functions on heavy atoms and p polarization functions on the hydrogen atoms basis set) level. To determine the harmonic force constants of the internal potential energy terms in the gas phase, we calculated the bond, angle, and dihedral potential energy curves of isolated NTO. From these potential energy curves, force constants k_b, k_θ, and k_ω could be evaluated by changing the bond length, bond angle, and improper angle by minute values around the optimized value. The force constant for the dihedral angle (k_Φ) was determined from the difference in the potential energy between the minimum and maximum in the range of 0−180°. The force constants of NTO are listed in Table 1. The equilibrium values of the bond lengths and bond angles (l_0 and θ_0, respectively) were determined by full geometry-based optimization. Partial atomic charges for NTO were calculated for a single isolated molecule with the optimized geometry by using the Merz−Kollman−Singh (MK) scheme except for the charges for the atoms involved in the hydrogen bond [N(2)−

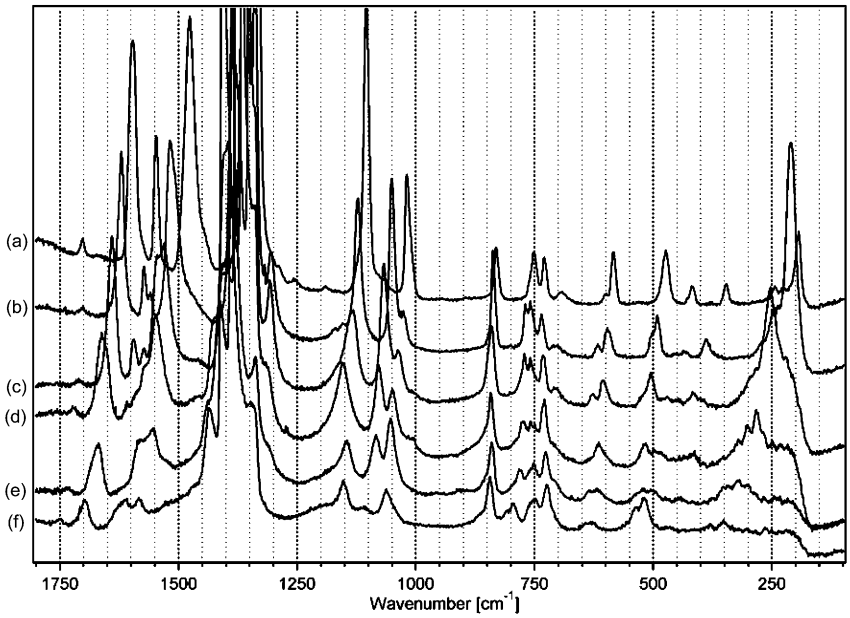

Figure 4. Effect of pressure on NTO in Raman spectra, in the high-pressure region: (a) 0, (b) 5.86, (c) 11.6, (d) 16.0, (e) 21.9, and (f) 27.6 GPa. Pressure values are represented as gauge pressure.

H(10)···O(9)═C(3)], which were precisely adjusted by the iterative calculation of the molecular dynamics simulations to maintain the ribbon structure of the α-NTO crystal. The obtained values are given in Table 2.

4. Results and Discussion

A. Raman Spectra of NTO in DAC. The Raman spectra of NTO under various pressure conditions are shown in Figures 3 and 4. There was a change in the relative intensity of the Raman bands due to the orientation of the CRYSTAL (not the orientation of a molecule in a crystal) in each series of experiments. It was impossible to control the direction of the ca. 50 μm length of the crystal in a hole which was 200 μm in diameter. Nevertheless, no frequency deviations were observed under the same conditions under repetitious measurements. In this work, the reproducibility of the Raman frequencies was good despite the fact that the intensity pattern exhibited several variations.

Some pressure effects were observed as frequency shifts. Generally, when the pressure increases further, molecules in the crystal are packed tightly, and the Raman bands are expected to exhibit blue shifts due to the decrease in the bond distance. However, as shown in Figures 3 and 4, some Raman bands of NTO did not move and some shifted to lower frequencies. Furthermore, some bands disappeared, and some new bands were found as the pressure increased. The vibrational assignment of this compound was accomplished in our previous study,[30] and therefore, it was possible to analyze the pressure effect on the particular structure of the molecule.

The normal phenomenon, a blue shift, can be categorized as one of three types in the pressure range of 0−27.6 GPa: (1) a simple blue shift, (2) a complicated blue shift, and (3) a slight shift. The simple blue shift phenomenon means an increase in the wavenumber as the pressure increases. In Figure 5, markers colored dark blue denote simple blue shifts that change frequencies linearly with pressure. The data for the complicated blue shift are colored light blue in Figure 5. The slopes of these blue shifts change at 3, 5−7, and 10−12 GPa. Mostly, the change in slope at 3 GPa related to splitting of Raman bands. At 5−7 GPa, the frequencies of some complicated blue-shifting bands stopped increasing. One can interpret that the spectral changes in these pressure ranges such as 3, 5−7, and 10−12 GPa show a change in the crystal lattice condition. For a further understanding of the NTO transition caused by static pressure, it is necessary to obtain X-ray diffraction data. However, the Raman spectrum pattern changes in the low-frequency region show the possibility of transition. An interesting phenomenon was observed at mode 11 (728 cm^{-1} at 0 GPa). This band shifted to a higher frequency as the pressure increased to 5 GPa, and then it started to exhibit a red shift at >5 GPa. This mode is assigned as ring deformation out of plane; in particular, this vibration has a strong contribution of carbon from the carbonyl group.[30] This fact implies that the carbonyl group plays an important role in the intermolecular condition in the crystal. According to our previous assignment, the bands (347, 600, 691, 1018, 1104, 1545, 1548, and 1599 cm^{-1} at 0 GPa) in group 2 exhibit a large blue shift related to ring stretching and NO_2 stretching. The slightly shifting bands in group 3 (751, 830, 1286, and 1332 cm^{-1} at 0 GPa) contained ring deformation motion. The stronger pressure effect was observed at nitro group-related bands. There was one more interesting blue-shifting band at 1255 cm^{-1} at 0 GPa. The intensity of this band decreased with compression and disappeared when the pressure reached ∼3 GPa. In our previous work, this band was not assigned by computational analysis; nevertheless, from the experimental data with isotope-labeled isomers, this band was related to NO_2, N(1) and N(2), and NH. A similar phenomenon was observed on the N(4)−H(11) stretching band at 3241 cm^{-1} at 0 GPa. The pressure effect on this N(4)−H(11) stretching band was red shifting, different from the 1255 cm^{-1} vibration, but it disappeared at 3 GPa just like that at 1255 cm^{-1}. These two disappearing bands exhibited a drastic change of N(4)−H(11) motion.

There were some unique effects with increasing pressure other than blue shifts, such as a red shift. The Raman bands at 1190 and 3192 cm^{-1} related to the NH group exhibited a red shift. In particular, the latter was a N(2)−H(10) stretching mode and shifted to a lower frequency by more than 70 cm^{-1} at 7 GPa with compression, and the intensity of this band was weakened as the pressure increased, as shown in Figures 5 and 6. Above

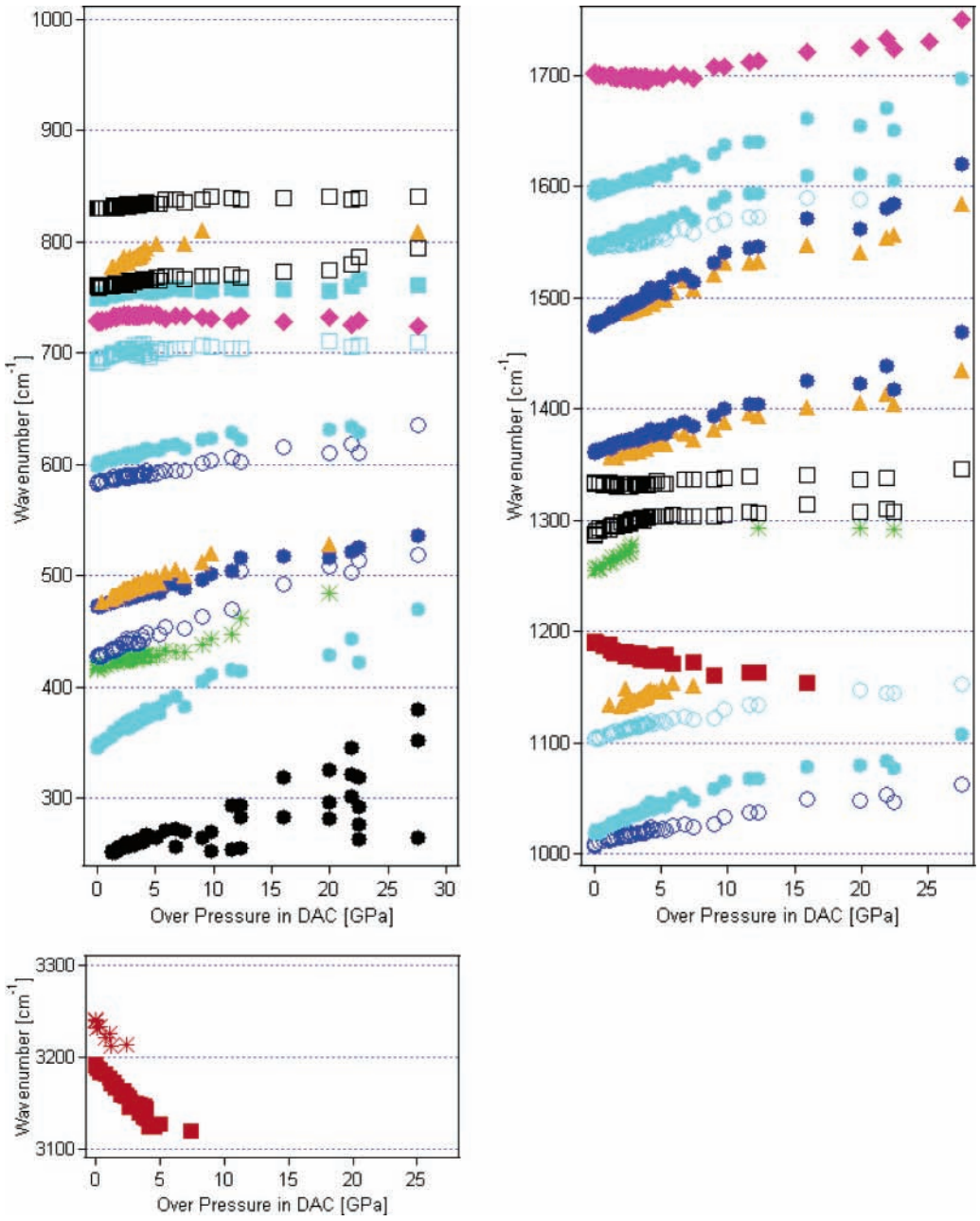

Figure 5. Effect of pressure on frequency shifts of NTO Raman bands: (dark blue circles) simple blue shift, (light blue circles) complicated blue shift, (black squares) slight blue shift, (orange triangles) newly observed bands, (red squares and asterisks) red shift, (asterisks) disappear, and (red diamonds and black circles) other.

10 GPa, this N(2)−H(10) stretching mode could not be observed due to the intensity decreasing and broadening. The other N(4)−H(11) stretching mode was found at 3241 cm^{-1}. It moved to a lower frequency with an increase in pressure, and its intensity decreased drastically as well. When the pressure increased to around 3 GPa, this N(4)−H(11) vibration could not be observed as described above.

The unique phenomenon was found on the C═O stretching mode (1702 cm^{-1} at 0 GPa) as shown in Figures 7 and 8. This frequency decreased with an increase in pressure to 3 GPa; therefore, the frequency did not change until 4 GPa, and then it started to show a blue shift at 5 GPa and continued to increase in frequency with compression. The intensity of the C═O stretching mode was weakened with compression until 5 GPa and recovered slightly when it started to move to a higher frequency (Figure 8). In general, hydrogen bond-related bands exhibit a red shift with an increase in pressure. It is natural that these bands related to N−H stretching and the C═O stretching of NTO represent the hydrogen bond from the shifting pattern with an increase in pressure. After compression to ca. 4 GPa, the hydrogen bond effect decreased at the C═O bond, and the length of the C═O bond started to be shortened with further compression. This phenomenon implies that the effect of intermolecular packing is not strong up to 5 GPa compared to intramolecular compression because the C−O distance is likely to be extended with a pressure increase to 5 GPa. This shows there is enough space outside of the NTO molecule in a crystal up to 5 GPa to release the strain from compression.

This motion seems to be a "tug of war" between oxygen and hydrogen (C−O···H). The basic research of the effect of pressure on the hydrogen bond of H_2O and ice in DAC was reported by Aoki et al.[39] The hydrogen bond in ice became stronger, and the O−H bond length was extended with compression. Finally, the symmetrization of the hydrogen bond

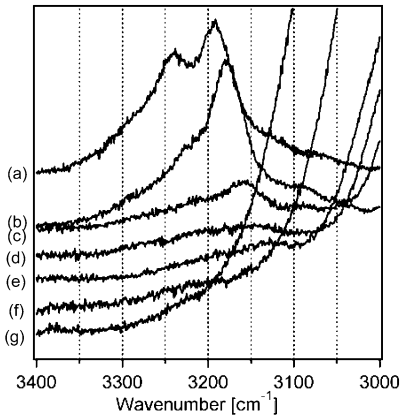

Figure 6. Effect of pressure on NTO N−H stretching in Raman spectra: (a) 0.05, (b) 1.10, (c) 2.36, (d) 3.45, (e) 4.60, (f) 6.74, and (g) 9.75 GPa. Pressure values are represented as gauge pressure.

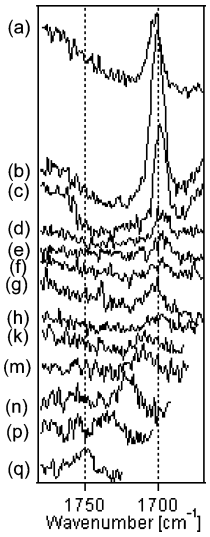

Figure 7. Effect of pressure on NTO carbonyl (C═O) stretching in Raman spectra: (a) 0, (b) 0.05, (c) 1.10, (d) 2.36, (e) 3.45, (f) 4.60, (g) 5.86, (h) 6.74, (k) 9.75, (m) 11.6, (n) 16.0, (p) 21.9, and (q) 27.6 GPa. Pressure values are represented as gauge pressure.

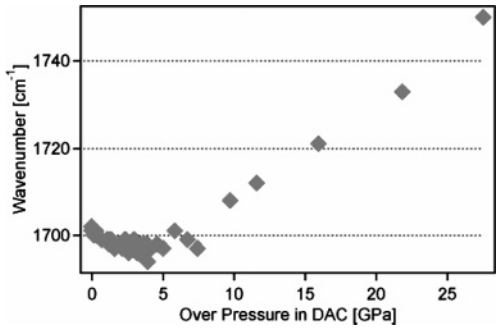

Figure 8. Frequency shift of NTO carbonyl (C═O) stretching with pressure in Raman spectra.

occurred. Our experimental condition is different from Aoki's work; however, a similar effect or tendency of the hydrogen bond might be observed on NTO with compression to 3 GPa. In this low-pressure region, a significant structural change such as a phase transition is likely to take place, since the shift of the C═O stretching exhibited different behavior in a higher-pressure region.

On comparison of NTO and a series of nitro aromatic compounds such as 2,4,6-trinitrotoluene (TNT), we confirmed that there were no obvious red-shifting Raman bands on TNT

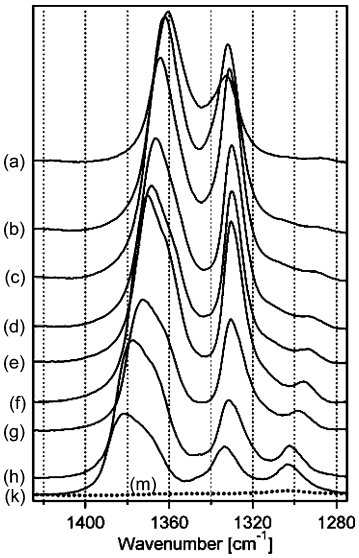

Figure 9. Effect of pressure on NTO in Raman spectra using the SiC anvil cell: (a) 0, (b) 0.30, (c) 0.71, (d) 1.23, (e) 1.62, (f) 2.16, (g) 2.58, (h) 3.89, and (k) 5.04 GPa and (m) background. Pressure values are represented as gauge pressure.

with compression such as C═O stretching of NTO; i.e., TNT is unlikely to show the hydrogen bond. The compounds which clearly exhibited a red shift were 1,3,5-triamino-2,4,6-trinitrobenzene (TATB) and 1,3-diamino-2,4,6-trinitrobenzene (DATB). This experimental result supports our theory about the correlation of the hydrogen bond and difficulty of the initiation of chemical reaction, i.e., insensitivity of explosives. Investigation of other aromatic nitro compounds is being undertaken in our other project. It will be reported in the near future.

The strong peak of the diamond anvil was observed at 1333 cm^{-1} at ambient pressure. It shifted to a higher frequency when the pressure increased and overlapped with some bands from NTO. To clarify the spectral change of this region, a SiC anvil was used, and good spectra were obtained without background interference, as shown in Figure 9. There is a Raman band from NTO at 1332 cm^{-1} at 0 GPa, and it hardly moved with compression.

There was a drastic change around 2−3 GPa in the spectral pattern, i.e., the relative intensities of each Raman band, especially in the low-frequency range, as seen in Figure 3. The intensities of most of the Raman bands in this region such as those at 347, 473, 585, and 729 cm^{-1} at 0 GPa decreased as the pressure increased. The Raman frequencies lower than ca. 300 cm^{-1} are supposed to correlate with phonon signals, i.e., the lattice structure. The spectral pattern change implies that there was a crystal lattice modification with compression.

Some bands that have shoulders such as 473, 1018, and 1545 cm^{-1} (with 1548 cm^{-1} at the shoulder) at 0 GPa started to split at the same time the intensity pattern change began. This phenomenon presents a decoupling of vibrations, observed as new peaks. The color of the NTO crystal changed with compression under the microscopic view. At ambient pressure, the NTO crystal was colorless or pale yellow. Once the crystal was pressurized, the NTO crystal became yellowish, and when the pressure load achieved the higher pressure, the crystal turned amber. This shows the change in the electronic properties or phase transition of the NTO crystal, not the reaction, since the crystal color becomes lighter when pressure is released, and the Raman spectrum was almost the same as before the compression.

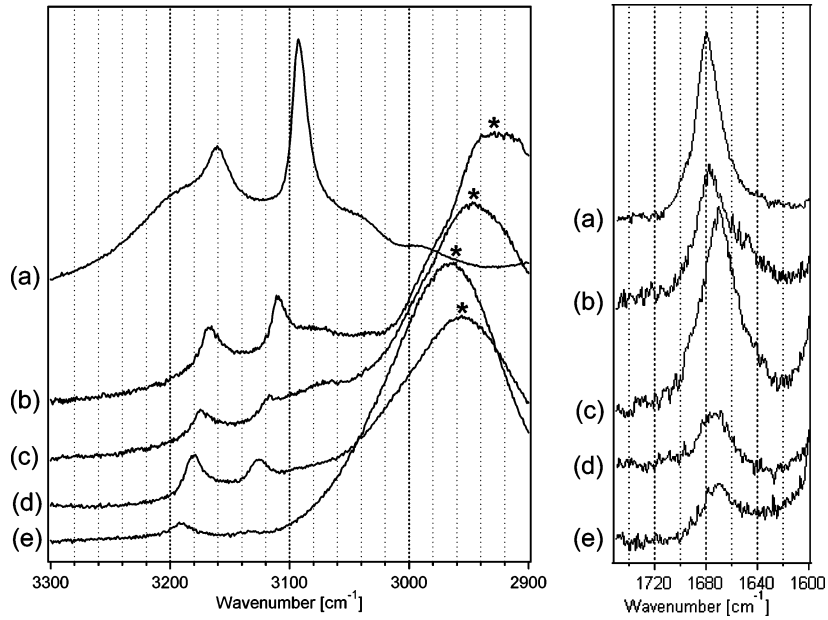

Figure 10. Effect of pressure on TO carbonyl stretching and N−H stretching in Raman spectra: (a) 0, (b) 1.37, (c) 2.96, (d) 4.38, and (e) 6.22 GPa and background. Pressure values are represented as gauge pressure. Asterisks indicate background based peaks.

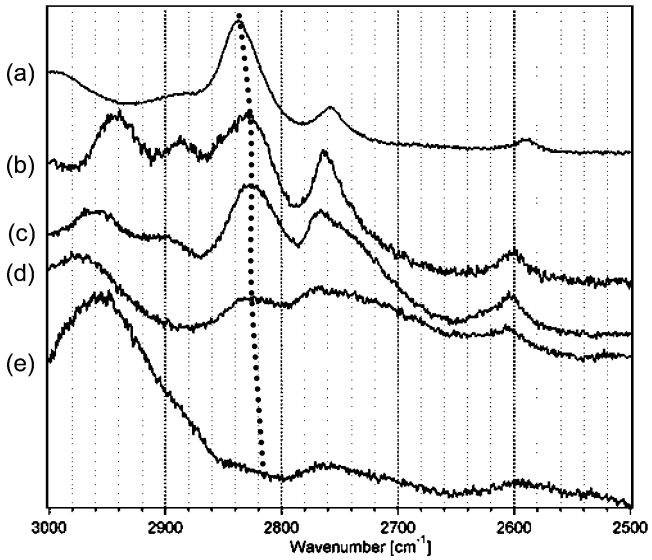

Figure 11. Effect of pressure on TO C−H stretching in Raman spectra (background subtracted): (a) ambient pressure and (b) 1.37, (c) 2.96, (d) 4.38, and (e) 6.22 GPa. Pressure values are represented as gauge pressure; dashed line indicates red shifting of C−H stretching with a pressure increase.

B. Effect of Nitro and Carbonyl Groups. TO, NTz, and Tz have a five-membered ring similar to that of NTO. The Raman spectra of TO, NTz, and Tz in DAC were also measured to investigate the effect of functional groups such as nitro and carbonyl groups.

In Figure 10, the Raman spectra of TO are given, and they clearly exhibit a red shift with a C═O stretching mode (1671 cm^{-1} at 0 GPa) as well as a NTO carbonyl mode (1702 cm^{-1} at 0 GPa); however, the N−H stretching mode of TO (3091 and 3158 cm^{-1} at 0 GPa) moved to a higher frequency while NTO exhibited a red shift. When the background was subtracted from the TO raw data, some weak broad bands could be seen in the 2500−3000 cm^{-1} region as shown in Figure 11, and that at 2837 cm^{-1} at ambient pressure is likely to show a red shift with an increase in pressure. The 2837 cm^{-1} band may possibly be C−H stretching, having a hydrogen bond with the carbonyl group.

On the other hand, NTz and Tz did not show any red shifts due to the deficiency of functional groups for the hydrogen bond. All of the Raman bands exhibited a blue shift, which implies that NTz and Tz were simply "compressed" as the pressure increased. These experimental results infer that a carbonyl group is necessary for the generation of an intermolecular hydrogen bond and that the oxygen atom in the nitro group cannot have a hydrogen bond with a hydrogen from the CH group, as seen in NTz.

The vibrational frequencies with regard to the NO_2 stretching of the NTO nitro group were lower than those of NTz; for example, NO_2 symmetric stretching-related vibrations were observed at 1360 cm^{-1} in NTO and 1425 cm^{-1} in NTz at 0 GPa. The hydrogen bond led by the carbonyl group in NTO is likely to make nitro group vibrations softer compared to that of NTz and cause a decrease in frequency.

These results prove that the hydrogen bond plays an important role in insensitiveness, and sometimes the hydrogen bond brought about the molecular and crystalline structural change as observed in the nitro group.

C. Crystal Structure of α-NTO. Crystallographic data and the results of the measurement are summarized in Table 3. There are eight molecules in the unit cell (Figure 12) with a density of 1.908 g/cm^3 (D_{cal} = 1.903 g/cm^3). The NTO molecules are joined by hydrogen bonds to form a ribbon structure of NTO molecules[8] (Figure 13). This ribbon of NTO molecules is duplicated by the center of symmetry at the origin to give a parallel ribbon. The horizontal direction is one of the axes of the crystal, and this repetitive distance is 5.134 Å. The ribbons of the NTO molecules consist of a two-dimensional hydrogen bond network. The layers of the ribbons are connected to each other by a relatively weak van der Waals force. Thus, the crystal structure obtained from the X-ray diffraction analysis was used for our MD calculations to build a crystal model.

D. Molecular Dynamics (MD). The crystal structure of α-NTO was used in all simulations. The system consists of 16 molecules in a two-unit cell. All simulations were performed

TABLE 3: Summary of Crystal Data for α-NTO

empirical formula	$C_2H_2N_4O_3$
formula weight	130.06
crystal color, habit	colorless, prismatic
crystal size (mm)	0.32 × 0.28 × 0.25
crystal system	triclinic
space group	$P\bar{1}$ (#2)
lattice parameters	
a (Å)	5.1343(6)
b (Å)	10.338(1)
c (Å)	18.023(2)
α (deg)	106.577(9)
β (deg)	97.61(1)
γ (deg)	90.30(1)
V (Å^3)	907.9(2)
Z value	8
D(calcd) (g/cm^3)	1.903
F_{000}	528.00
μ (Mo *K*α) (cm^{-1})	1.76
no. of reflections measured	5035
no. of independent reflections	4969 (R_{int} = 0.059)
no. of variables	357
reflection/parameter ratio	13.92
residuals (R_1,[a] R_w[b])	0.064, 0.181[d]
no. of reflections to calculate R_1	4082 [$I > 2.0\sigma(I)$]
goodness of fit indicator[c]	1.29[d]
maximum peak in the final difference map (e/Å^3)	0.46
minimum peak in the final difference map (e/Å^3)	−0.41

[a] $R = \sum||F_o| - |F_c||/\sum|F_o|$ for observed data. [b] $R_w = [\sum w(F_o^2 - F_c^2)^2/\sum w(F_o^2)^2]^{1/2}$ for all data. [c] GOF = $[\sum w(|F_o| - |F_c|)^2/(N_o - N_v)]^{1/2}$. [d] $w = [\sigma^2(F_o^2) + (0.0426P)^2 + 2.1606P]^{-1}$, where $P = (F_o^2 + 2F_c^2)/3$.

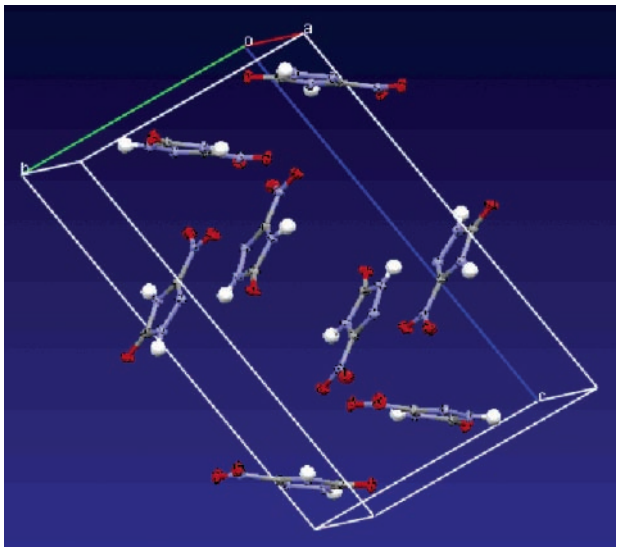

Figure 12. Unit cell of the α-NTO crystal with the thermal ellipsoid drawn at the 50% probability level.[36] Carbon, nitrogen, oxygen, and hydrogen atoms are colored gray, blue, red, and white, respectively.

in the NPT ensemble (constant number of molecules, pressure, and temperature). Periodic boundary conditions were enforced by creating images of the atoms in the primary simulation cell (two-unit cell). The lattice parameters and atomic coordinates are minimized together before the molecular dynamics calculation. It should be noted that when the lattice was being optimized, crystal symmetry was maintained.

Molecular dynamics simulations were performed by classical mechanics. Initial velocities for all atoms in these systems were selected at random from a Boltzmann distribution at 300 K. Newton's equation of motion was then integrated by using a Verlet integrator with a step size of 0.1 fs, and the nonbonded neighbor list was updated every 20 steps.

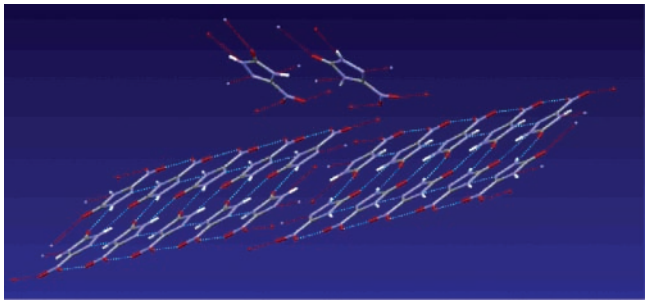

Figure 13. Ribbon structures of NTO molecules and short contact atoms.[36] Carbon, nitrogen, oxygen, and hydrogen atoms are colored gray, blue, red, and white, respectively.

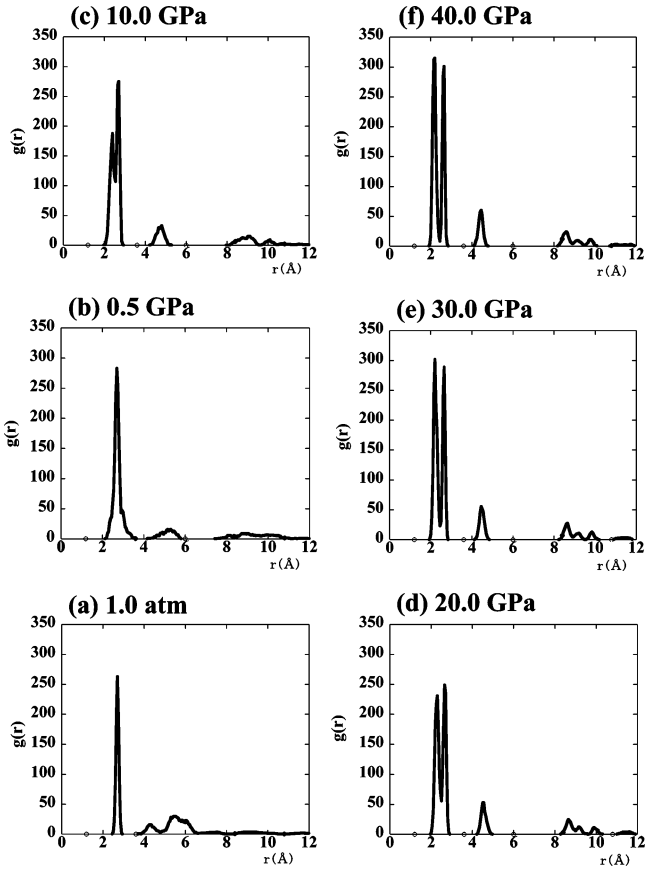

Figure 14. Typical radial distribution functions (RDFs) for C═O(9)···H(10)−N pairs (including the hydrogen bond) in the primary simulation cell as functions of pressure. There are six RDFs (pairs) in the primary simulation cell. These RDFs are almost the same.

In the initial simulation corresponding to the condition at 300 K and 1.0 atm, the position and orientation of the molecules in the unit cell were taken to be identical to those for the experimental structure. After equilibration for 40 ps at 1.0 atm and 300 K, an analysis run of the 10 ps MD calculation was performed from 1.0 atm to 50.0 GPa by increasing the pressure every 0.5 GPa. The changes in the H(10)···O(9) and C═O(9) bond lengths were plotted as functions of time. The radial distribution functions (RDFs) for the C═O(9)···H(10)−N pairs were analyzed as functions of distance. In addition, to analyze the characteristic wave pattern in the simulations, we calculated the autocorrelation functions and power spectra by using CHARMM29. The first 6 ps of all the 10 ps trajectories was used in the calculation of the correlation functions. The power spectra were obtained from the Fourier transform of the correlation function.

TABLE 4: Pressure Dependence of the Lengths of the Six Hydrogen Bond Pairs for the Same H(10)···O(9) Bond and the Length of the C═O(9) Bond in the α Form Crystal

bond no.	1.0 atm	0.5 GPa	5.0 GPa	10.0 GPa	15.0 GPa	20.0 GPa	30.0 GPa	40.0 GPa	50.0 GPa
O···H;1	3.021	2.707	2.503	2.321	2.273	2.220	2.275	2.129	2.259
O···H;2	3.327	2.494	2.349	2.404	2.261	2.346	2.204	2.366	2.197
O···H;3	2.843	2.325	2.684	2.390	2.301	2.117	2.233	2.286	2.136
O···H;4	2.713	3.575	2.185	2.258	2.215	2.224	2.239	2.279	2.278
O···H;5	3.259	2.687	2.429	2.459	2.429	2.384	2.172	2.238	2.159
O···H;6	2.930	2.420	2.486	2.378	2.431	2.157	2.183	2.247	2.248
mean	3.016	2.701	2.439	2.368	2.318	2.241	2.218	2.258	2.213
C═O;1	1.180	1.192	1.191	1.198	1.208	1.181	1.191	1.148	1.181
C═O;2	1.208	1.200	1.175	1.182	1.212	1.167	1.194	1.155	1.172
C═O;3	1.190	1.209	1.187	1.165	1.171	1.182	1.175	1.159	1.170
C═O;4	1.173	1.183	1.217	1.195	1.215	1.224	1.167	1.169	1.138
C═O;5	1.204	1.182	1.188	1.235	1.195	1.167	1.176	1.171	1.192
C═O;6	1.192	1.207	1.209	1.227	1.222	1.177	1.175	1.197	1.183
mean	1.191	1.196	1.195	1.200	1.204	1.183	1.180	1.167	1.173

TABLE 5: Calculated and Experimental Vibrational Frequencies of α-NTO

		calcd (this work by CHARMM29)[a]		B2LYP/6-311++G(2df,2pd)[30]		IR frequency[30]	Raman frequency[30]
mode	assignment[30]	calcd	scaled[40,41]	calcd	scaled[42]	exptl	exptl
1	ring-NO_2 def. out of plane	221.7	141.7	83.9	80.6		122
2	ring def. + ring-NO_2 def. out of plane	303.2	178.5	144.4	138.8		192
3	ring-NO_2 def. in plane	318.2	239.2	202.6	194.8		277/243
4	ring def. + ring-NO_2 out of plane	432.0	342.0	306.6	294.7		347
5	C−NO_2 stretch + C−O def. out of plane	571.5	428.1	405.5	389.8		418
6	NO_2 def. + ring-NO_2 def. + C−O def. in plane	602.5	455.6	463.8	445.8		427
7	N−H def. + ring def. out of plane	686.4	545.3	489.6	470.6		473
8	N−H def. + ring def. out of plane	807.4	625.2	542.8	521.8		585
9	ring-NO_2 def. + C−O def. in plane	824.7	653.8	581.9	559.4		600
10	ring def. out of plane	863.2	686.6	657.9	632.4	682	691
11	ring def. out of plane	970.3	749.5	745.9	717.0	731	729
12	ring def. + NO_2 def. in plane	1053.1	832.4	752.9	723.8	750	751
13	ring def. + ring-NO_2 def. out of plane	1099.3	874.3	782.2	752.0	787	
14	ring def. + NO_2 def. in plane	1200.8	915.2	839.9	807.4	829	830
15	ring def. + N−H def. in plane	1218.7	970.6	982.5	944.5	1006	1009
16	ring def. + N−H def. + ring-NO_2 stretch in plane	1328.7	1040.5	1009.2	970.2	1018	1018
17	ring def. (N1−N2−C3 asymmetric stretch) in plane	1439.2	1148.4	1085.1	1043.2	1109	1104
18	ring def. + N−H def. in plane	1495.3	1156.1	1206.9	1160.2	1188	1190
19	ring def. + N−H def. in plane	1576.4	1256.3	1266.0	1217.0	1280	1286
20	NO_2 def + NO_2 symmetric stretch + N−H def. in plane	1650.7	1317.1	1366.0	1313.2	1355	1360
21	N−H def. + ring def. in plane	1725.6	1381.6	1389.5	1335.8	1340	1332
22	ring def. + N−H def. + NO_2 def. in plane	1844.7	1468.8	1465.9	1409.2	1473	1475
23	ring def. + NO_2 asymmetric stretch in plane	1965.1	1568.2	1596.4	1534.7	1541	1545
24	ring def. + NO_2 asymmetric stretch in plane	2011.4	1602.2	1625.3	1562.4	1546	1548
25	C═O stretch	2228.5	1770.1	1839.8	1768.6	1691/1712	1702
26	N2−H10 stretch	3678.1	2940.1	3659.2	3517.6	3198	3192
27	N4−H11 stretch	3683.7	2944.2	3660.1	3518.4	3242	3241

[a] Force constants, etc., were obtained by B3LYP/6-311++G(d,p) level calculations.

1. Radial Distribution Functions. The radial distribution functions for the C═O(9)···H(10)−N pairs (including the hydrogen bond) as functions of pressure were calculated and are shown in Figure 14. For a NTO molecule in the α form crystal structure at 1.0 atm, the first, second, and third shells of neighbor atoms are within a radius of approximately 2.7, 5.0, and 6.5 Å, respectively. When the pressure increased to 10.0 GPa, a new first shell of neighbor atoms (i.e., a new peak) appeared within a radius of ca. 2.4 Å, while other peak intensities did not change. Thus, the splitting of the main peak in the 2−3 Å region represents the existence of different interactions. Each peak corresponds to an intramolecular O(9)···H(11) separation in the NTO molecule and an intermolecular O(9)···H(10) (hydrogen bond) separation in a ribbon of NTO molecules. MD calculations were also carried out with the pressure at (d) 20.0, (e) 30.0, and (f) 40.0 GPa. The position of the new peak was located in ca. (d) 2.3, (e) 2.2, and (f) 2.2 Å, respectively. The hydrogen bond lengths at various pressures from 1.0 atm to 50.0 GPa are listed in Table 4. As our simulation box consists of 16 molecules in a two-unit cell, there are six hydrogen bond pairs for the same O(9)···H(10) interaction in these cells. These pairs are numbered as O···H;1, O···H;2, ..., O···H;6 arbitrarily in Table 4. The O(9)···H(10) hydrogen bond length was evaluated by simply averaging all the hydrogen bond lengths in Table 4. Thus, these distances corresponded to a hydrogen bond [H(10)···O(9)] separation in a ribbon of NTO molecule as the pressure increased. When the pressure increases, hydrogen bond lengths [H(10)···O(9)] become gradually shorter. However, a particular high-pressure effect of the α-NTO crystal was found on the C═O bond length. This bond length increased with the degree of compression up to 15.0 GPa. However, when the pressure increased more than 20.0 GPa, the C═O bond length became gradually shorter along with the hydrogen bond distance. These theoretical results are in agreement with the experimental results given in the previous section. This will be discussed in detail below.

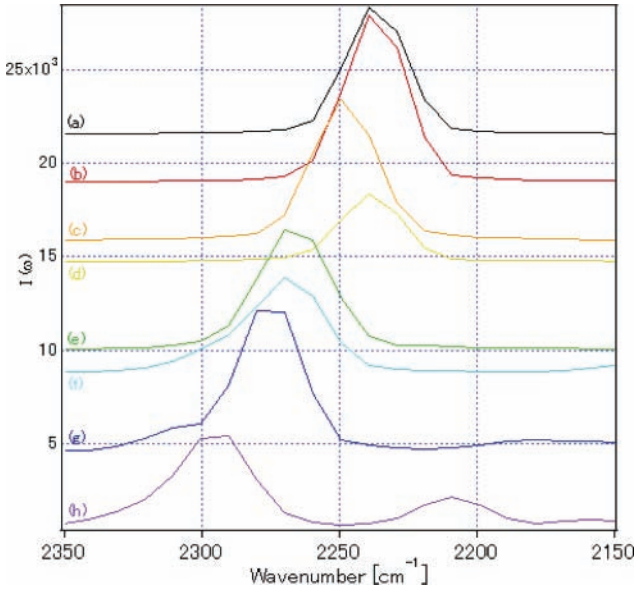

Figure 15. Pressure dependence of the power spectra of the correlation functions of C═O bond length in NTO: (a) 1.0 atm and (b) 0.50, (c) 5.0, (d) 10.0, (e) 20.0, (f) 30.0, (g) 40.0, and (h) 50.0 GPa.

2. Vibrational Frequencies. The calculated and observed vibrational frequencies of the α-NTO crystal are compared in Table 5. The agreement was satisfactory overall, although the difference in two instances (N−H stretching mode) was more than 200 cm^{-1}. Figure 15 shows the pressure dependence of the power spectra of the correlation functions of the C═O bond length in NTO. The peak in the power spectra of the C═O stretching vibration exhibited a blue shift as the pressure increased in the range of 20.0−50.0 GPa. A blue shift appeared when the pressure was considerably increased, since high pressure makes the bond distance shorter. At a pressure higher than 20.0 GPa, the C═O bond length became shorter (Table 4). On the other hand, an unusual high-pressure effect of the α-NTO crystal was also found on the power spectra of the correlation functions of the C═O bond length. The peak frequency in the power spectrum of the C═O stretching vibration decreased with an increase in pressure to 10.0 GPa except at 5.0 GPa, while the peak intensity considerably decreased because this bond length increased with an increase in pressure to 10.0 GPa. On the other hand, when the pressure increases range from 0.5 to 5.0 GPa, the C═O bond length (C═O;1, C═O;2, ..., C═O;6) shows some scatter as shown in Table 4. The mean values at 0.5 and 5.0 GPa are approximately equivalent (1.196 and 1.195 Å, respectively). The peak frequency in the power spectrum of the C═O stretching vibration at 5.0 GPa is influenced by the pressure conditions. Therefore, these results of MD calculations were in good agreement with our experimental data. These results strongly suggest that carbonyl groups are likely to work as a sort of stabilizer against external stimuli (e.g., heat or impact) to the NTO molecule before the beginning of the decomposition reactions of the α-NTO crystal. Thus, the hydrogen bond related to the carbonyl group played an important role in the molecular structural relaxation with an increase in pressure.

5. Conclusions

The Raman spectra of NTO at high pressures were obtained. There were some unique shifts rather than ordinary blue shifts. Interesting pressure effects were strongly observed on carbonyl (C═O), N−H, and some ring deformation vibrations. From the results of the pressure effect on the carbonyl and hydrogen bond, intermolecular packing is not strong up to 5 GPa compared to intramolecular compression, because the bond order of the C−O bond decreased as the Raman frequency exhibited a red shift; i.e., a C−O distance was extended with the pressure increase. This partial structural change means there is enough space outside of the molecule itself to release the strain from compression, and possibly stabilize the structure of NTO. MD calculations supported these experimental results, especially the unique shifting of the carbonyl. These results indicated that this property of NTO with respect to the pressure stimuli is based on the ribbon structure of the α-NTO crystal. It was predicted that the hydrogen bond related to the carbonyl group played an important role as a stabilizing system in the molecular structural relaxation with an increase in pressure and related to the insensitivity of explosives, such as a delay system of initiation of a chemical reaction. To the best of our knowledge, the interesting effect on Raman spectra related to the hydrogen bond was experimentally shown for the first time.

Acknowledgment. The DFT computations were performed using the Research Center for Computational Science (Okazaki, Japan). We are also very grateful to the late Noriaki Toyoshima of Kyowa Seisakusho for the devotion with which he handled the DAC. We are also grateful to the late Prof. Ko Saito of Hiroshima University for his deep consideration of, and helpful advice on, this work.

Supporting Information Available: X-ray crystallographic file (CIF) of α-NTO. This material is available free of charge via the Internet at http://pubs.acs.org.

References and Notes

(1) Williams, G. K.; Brill, T. B. *J. Phys. Chem.* **1995**, *99*, 12536−12539.
(2) Singh, G.; Kapoor, I. P. S.; Mannan, S. M.; Tiwari, S. K. *J. Hazard. Mater.* **1999**, *A68*, 155−178.
(3) Oxley, J. C.; Smith, J. L.; Rogers, E.; Dong, X. X. *J. Phys. Chem. A* **1997**, *101*, 3531−3536.
(4) Östmark, H.; Bergman, H.; Åaqvist, G.; Langlet, A.; Persson, B. *Proceedings of the 16th International Pyrotechnics Seminar*, Jönköping, Sweden, June 1991, pp 874−886.
(5) Sanderson, A. J. *NIMIC*, Sep 30, 1997.
(6) Piteau, M.; Becuwe, A.; Finck, B. *ADPA Symposium*; San Diego, CA, April 1991; pp 69−79.
(7) Becuwe, A.; Delclos, A. *Propellants, Explos., Pyrotech.* **1993**, *18* (1), 1−10.
(8) Lee Kien-yin; Gilardi, R. *Mater. Res. Soc. Proc.* **1993**, *295*, 237−242.
(9) Bolotina, N. B.; Zhurova, E. A.; Pinkerton, A. A. *J. Appl. Crystallogr.* **2003**, *36*, 280−285.
(10) Zhurova, E. A.; Pinkerton, A. A. *Acta Crystallogr.* **2001**, *B57*, 359−365.
(11) Ritchie, J. P. *J. Org. Chem.* **1989**, *54*, 3553−3560.
(12) Harris, N. J.; Lammertsma, K. *J. Am. Chem. Soc.* **1996**, *118*, 8048−8055.
(13) Sorescu, D. C.; Sutton, T. R. L.; Thompson, D. L.; Beardall, D.; Wight, C. A. *J. Mol. Struct.* **1996**, *384*, 87−99.
(14) Sorescu, D. C.; Thompson, D. L. *J. Phys. Chem. B* **1997**, *101*, 3605−3613.
(15) Meredith, C.; Russell, T. P.; Mowrey, R. C.; MacDonald, J. R. *J. Phys. Chem. A* **1998**, *102*, 471−477.
(16) Wang, Y. M.; Chen, C.; Lin, S. T. *THEOCHEM* **1999**, *460*, 79−102.
(17) Yim, W. L.; Liu, Z. F. *J. Am. Chem. Soc.* **2001**, *123*, 2243−2250.
(18) Kohno, Y.; Takahashi, O.; Saito, K. *Phys. Chem. Chem. Phys.* **2001**, *3*, 2742−2746.
(19) Hare, D. E.; Franken, J.; Dlott, D. D. *Chem. Phys. Lett.* **1995**, *244*, 224−230.
(20) Tsang, W.; Robaugh, D.; Mallard, W. G. *J. Phys. Chem.* **1986**, *90*, 5968−5973.
(21) Chen, S.; Hong, X.; Hill, J. R.; Dlott, D. D. *J. Phys. Chem.* **1995**, *99*, 4525−4530.

(22) Dick, J. J.; Mulford, R. N.; Spencer, W. J.; Pettit, D. R.; Garcia, E.; Shaw, D. C. *J. Appl. Phys.* **1991**, *70* (7), 3572−3587.

(23) Franken, J.; Hambir, S. A.; Dlott, D. D. *J. Appl. Phys.* **1999**, *85* (4), 2068−2074.

(24) Licht, H. *Propellants, Explos., Pyrotech.* **2000**, *25*, 126−132.

(25) Politzer, P.; Alper, H. E. In *Computer chemistry, Reviews of current trends*; Leszczynski, J., Ed.; World Scientific: Singapore, 1999; Vol. 4, Chapter 6.

(26) Alper, H. E.; Abu-Awward, F.; Politzer, P. *J. Phys. Chem. B* **1999**, *103*, 9738−9742.

(27) Sorescu, D. C.; Rice, B. M.; Thompson, D. L. *J. Phys. Chem. B* **1998**, *102*, 6692−6695.

(28) Kohno, Y.; Ueda, K.; Imamura, A. *J. Phys. Chem.* **1996**, *100*, 4701−4712.

(29) Oxley, J. C.; Smith, J. L.; Yeager, K. E. *J. Energ. Mater.* **1995**, *13*, 93−105.

(30) Hiyoshi, R. I.; Kohno, Y.; Nakamura, J. *J. Phys. Chem. A* **2004**, *108*, 5915−5920.

(31) Piermarini, G. J.; Block, S.; Barnett, J. D.; Forman, R. A. *J. Appl. Phys.* **1975**, *46* (6), 2774−2780.

(32) Altomare, A.; Burla, M. C.; Camalli, M.; Cascarano, M.; Giacovazzo, C.; Guagliardi, A.; Polidori, G. SIR 92. *J. Appl. Crystallogr.* **1994**, *27*, 435.

(33) Beurskens, P. T.; Admiraal, G.; Beurskens, G.; Bosman, W. P.; de Gelder, R.; Israel, R.; Smits, J. M. M., *DIRDIF 94: The DIRDIF-94 program system*; Technical Report of the Crystallography Laboratory; University of Nijmegen: Nijmegen, The Netherlands, 1994.

(34) Sheldrick, G. M., *SHELXL-97: Program for the Refinement of Crystal Structures*; University of Göttingen: Göttingen, Germany, 1997.

(35) *teXsan: Crystal Structure Analysis Package*; Molecular Structure Corp., 1985 and 2004.

(36) The diagram was drawn with Mercury 1.4 (http://www.ccdc.cam.ac.uk/mercury/).

(37) Brooks, B. R.; Bruccoleri, R. E.; Olafson, B. D.; States, D. J.; Swaminathan, S.; Karplus, M. *J. Comput. Chem.* **1983**, *4*, 187−217.

(38) Frisch, M. J.; Trucks, G. W.; Schlegel, H. B.; Scuseria, G. E.; Robb, M. A.; Cheeseman, J. R.; Zakrzewski, V. G.; Montgomery, J. A.; Stratmann, R. E., Jr.; Burant, J. C.; Dapprich, S.; Millam, J. M.; Daniels, A. D.; Kudin, K. N.; Strain, M. C.; Farkas, O.; Tomasi, J.; Barone, V.; Cossi, M.; Cammi, R.; Mennucci, B.; Pomelli, C.; Adamo, C.; Clifford, S.; Ochterski, J.; Petersson, G. A.; Ayala, P. Y.; Cui, Q.; Morokuma, K.; Salvador, P.; Dannenberg, J. J.; Malick, D. K.; Rabuck, A. D.; Raghavachari, K.; Foresman, J. B.; Cioslowski, J.; Ortiz, J. V.; Baboul, G.; Stefanov, B. B.; Liu, G.; Liashenko, A.; Piskorz, P.; Komaromi, I.; Gomperts, R.; Martin, R. L.; Fox, D. J.; Keith, T.; Al-Laham, M. A.; Peng, C. Y.; Nanayakkara, A.; Challacombe, M.; Gill, P. M. W.; Johnson, B.; Chen, W.; Wong, M. W.; Andres, J. L.; Gonzalez, C.; Head-Gordon, M.; Replogle, E. S.; Pople, J. A. *Gaussian 98*, revision A.11.1; Gaussian, Inc.: Pittsburgh, PA, 2001.

(39) Aoki, K.; Yamawaki, H.; Sakashita, M.; Fujihisa, H. *Phys. Rev. B* **1996**, *54* (22), 15673−15677.

(40) Woods, R. J.; Dwek, R. A.; Edge, C. J. *J. Phys. Chem.* **1995**, *99*, 3832−3846.

(41) MackKerell, A. D., Jr.; Bashford, D.; Bellott, M.; Dunbrack, R. L., Jr.; Evanseck, J. D.; Field, M. J.; Fischer, S.; Gao, J.; Guo, H.; Ha, S.; Joseph-McCarthy, D.; Kuchnir, L.; Kuczera, K.; Lau, F. T. K.; Mattos, C.; Michnick, S.; Ngo, T.; Nguyen, D. T.; Prodhom, B.; Reiher, W. E., III; Roux, B.; Schlenkrich, M.; Smith, J. C.; Stote, R.; Straub, J.; Watanabe, M.; Wiórkiewicz-Kuczera, J.; Yin, D.; Karplus, M. *J. Phys. Chem. B* **1998**, *102*, 3586−3616.

(42) Forseman, J. B.; Frisch, A. *Exploring Chemistry with Electronic Structure Methods*; Gaussian, Inc.: Pittsburgh, PA, 1996.